

Accommodation of Two Diatomic Molecules in Cytochrome *bo*₃: Insights into NO Reductase Activity in Terminal Oxidases[†]

Takahiro Hayashi,[‡] Myat T. Lin,[§] Krithika Ganesan,[§] Ying Chen,^{||} James A. Fee,^{||} Robert B. Gennis,[§] and Pierre Moënne-Loccoz^{*,‡}

Department of Science and Engineering, School of Medicine, Oregon Health & Science University, 20,000 NW Walker Road, Beaverton, Oregon 97006-8921, Departments of Biochemistry, University of Illinois, Urbana, Illinois 61801, and Department of Molecular Biology, The Scripps Research Institute, La Jolla, California 92037

Received October 11, 2008; Revised Manuscript Received December 16, 2008

ABSTRACT: Bacterial heme–copper terminal oxidases react quickly with NO to form a heme–nitrosyl complex, which, in some of these enzymes, can further react with a second NO molecule to produce N₂O. Previously, we characterized the heme *a*₃–NO complex formed in cytochrome *ba*₃ from *Thermus thermophilus* and the product of its low-temperature illumination. We showed that the photolyzed NO group binds to Cu_B(I) to form an end-on NO–Cu_B or a side-on copper–nitrosyl complex, which is likely to represent the binding characteristics of the second NO molecule at the heme–copper active site. Here we present a comparative study with cytochrome *bo*₃ from *Escherichia coli*. Both terminal oxidases are shown to catalyze the same two-electron reduction of NO to N₂O. The EPR and resonance Raman signatures of the heme *o*₃–NO complex are comparable to those of the *a*₃–NO complex. However, low-temperature FTIR experiments reveal that photolysis of the heme *o*₃–NO complex does not produce a Cu_B–nitrosyl complex, but that instead, the NO remains unbound in the active-site cavity. Additional FTIR photolysis experiments on the heme–nitrosyl complexes of these terminal oxidases, in the presence of CO, demonstrate that an [*o*₃–NO•OC–Cu_B] tertiary complex can form in *bo*₃ but not in *ba*₃. We assign these differences to a greater iron–copper distance in the reduced form of *bo*₃ compared to that of *ba*₃. Because this difference in metal–metal distance does not appear to affect the NO reductase activity, our results suggest that the coordination of the second NO to Cu_B is not an essential step of the reaction mechanism.

The reduction of nitric oxide (NO) to nitrous oxide (N₂O) (eq 1) is an obligatory step in the bacterial denitrification pathway which converts nitrate to atmospheric nitrogen.



Denitrifying NO reductases found in many prokaryotes, including symbiotic and pathogenic bacteria, have been shown to provide those microorganisms resistance to the mammalian immune response. For example, *Neisseria gonorrhoeae* and *Neisseria meningitidis*, the causative agents of meningococcal disease in humans, depend upon NO reductases to tolerate toxic concentrations of NO (1–3). These integral protein complexes contain a NorB subunit evolutionarily related to subunit I of heme–copper terminal oxidases (4, 5). There are no crystal structures available for NO reductases (NORs) yet, but sequence alignments and hydropathy plots suggest that the six histidine side chains involved in ligating metal cofactors in terminal oxidases are conserved in norB (6). While O₂ reduction in terminal

oxidases occurs at a heme–copper dinuclear site, the reduction of NO by NOR takes place at a heme–nonheme diiron center (7–11). Despite the difference in metal composition, several heme–copper terminal oxidases (i.e., *ba*₃, *bo*₃, and *cbb*₃) are capable of catalyzing the reduction of NO, albeit with much lower turnover rates compared to NORs (12–14). This low NO reductase activity is unlikely to be the primary function of these enzymes, but studying their interaction with NO can expand our knowledge of NO reduction mechanisms in NOR and, more generally, in dinuclear active centers.

The catalytic mechanism of NO reduction in terminal oxidases is generally considered to be initiated by the binding of NO to the high-spin heme in the fully reduced enzyme. Subsequent steps are expected to involve Cu_B, either as a coordination site for a second molecule of NO or as an electron donor and electrostatic partner to a heme–hyponitrite complex [Fe(III)–N₂O₂²⁻•Cu_B(II)] (11, 15–17). Vos and co-workers have monitored the rebinding kinetics of the photolyzed NO in *ba*₃–NO at room temperature and interpreted the lack of significant subnanosecond NO rebinding to heme *a*₃ as evidence of the photolyzed NO binding to Cu_B before rebinding to the heme *a*₃ (18). In our subsequent FTIR photolysis study of *ba*₃–NO at cryogenic temperature, we observed the formation of a Cu_B–nitrosyl species with an unusual N–O stretching frequency suggestive of an O-bound (η¹-O) or side-on (η²-NO) configuration (17). The

[†] This work was supported in part by the National Institutes of Health (P.M.-L., GM74785; J.A.F., GM35342) and the Department of Energy (R.B.G., DE-FG02–87ER13716).

* Corresponding author. Tel: 503-748-1673. Fax: 503-748-1464. E-mail: plocco@ebs.ogi.edu.

[‡] Oregon Health & Science University.

[§] University of Illinois.

^{||} The Scripps Research Institute.

characterization of this complex suggests that the N–N bond formation in ba_3 does not proceed from a transient $[a_3\text{--NO}\cdot\text{ON--Cu}_B]$ trans $ba_3\text{--(NO)}_2$ complex as proposed by Ohta and co-workers (15). Indeed, if an N-bound $\text{Cu}_B\text{--nitrosyl}$ was the species formed in the transient $ba_3\text{--(NO)}_2$ complex, one would expect the photoinduced $\text{Cu}_B\text{--nitrosyl}$ complex to adopt this geometry even in the absence of the heme $a_3\text{--NO}$ species nearby.

In light of these results, it is tempting to speculate that the photoinduced $\text{Cu}_B\text{--nitrosyl}$ species generated in $ba_3\text{--NO}$ describes the mode of binding of the second NO molecule. To determine whether the hypothesis drawn from the results with ba_3 applies to other terminal oxidases with NO reductase activity, we now direct our work to the bo_3 quinol oxidase from *Escherichia coli*. A few investigations have been focused on the interaction of NO with bo_3 from *E. coli*. Sarti and co-workers measured a low but significant NO reductase activity in bo_3 under reducing conditions (14). On the basis of EPR data, Thomson and co-workers have proposed that two NO molecules bind to $\text{Cu}_B(\text{II})$ in the oxidized form of bo_3 (19). To our knowledge, cytochrome bo_3 is the only quinol oxidase reported to exhibit NO reductase activity, and as such, it provides a relevant model for the quinol NOR (qNOR) from *N. gonorrhoeae* and *Neisseria meningitidis* (3).

Here we report cryogenic FTIR photolysis experiments on fully reduced $bo_3\text{--NO}$ and the mixed gas $bo_3\text{--CO/NO}$ complexes. Amperometric measurements of NO concentrations and monitoring of N_2O production by FTIR spectroscopy demonstrate that ba_3 and bo_3 catalyze the same reaction at similar rates. However, the $\text{Cu}_B\text{--nitrosyl}$ species observed in $ba_3\text{--NO}$ does not form in $bo_3\text{--NO}$. Instead, the photolyzed NO of the latter docks at a protein pocket that leads to efficient NO geminate recombination similar to that in ferrous myoglobin–NO (20). FTIR experiments, carried out on ba_3 and bo_3 exposed to NO/CO mixed gas, show concomitant binding of two diatomic molecules only in the dinuclear site of bo_3 to form an $[o_3\text{--NO}\cdot\text{OC--Cu}_B]$ tertiary complex. The relevance of this $[o_3\text{--NO}\cdot\text{OC--Cu}_B]$ state to the NO reductase activity in cytochrome bo_3 is discussed in the context of other terminal oxidases and of denitrifying NO reductases.

MATERIALS AND METHODS

Protein Stock Solutions. The expression and purification of aa_3 , ba_3 and bo_3 were performed as previously described (21, 22). For all experiments, cytochrome aa_3 and ba_3 were in 50 mM potassium phosphate pH 7.4 and 0.1% dodecyl β -D-maltoside, and 20 mM Tris-HCl pH 7.5 with 0.05% dodecyl β -D-maltoside, respectively. Cytochrome bo_3 was in 50 mM potassium phosphate pH 8.0 with 0.1% dodecyl β -D-maltoside, 10 mM EDTA, and 5% glycerol.

NO Reductase Activity Measurements. NO stock solutions were prepared by bubbling NO gas, previously treated with 1 M KOH, into double-distilled water in an anaerobically sealed vessel for ~ 15 min at 25 °C. The concentration of NO in the solution was determined to be 1.5 mM by titration against ferrous Mb. NO reduction measurements were carried out with a Clark-type NO electrode equipped with a 2 mL gastight sample chamber at 20 °C in a glovebox containing less than 1 ppm of O_2 (Omnilab System, Vacuum Atmospheres Company). The current was stabilized with a buffer

solution containing 10 mM ascorbate and 0.1 mM N,N,N',N' -tetramethyl-*p*-phenylenediamine (TMPD) in the sample chamber, followed by three successive additions of saturated NO solution to reach final NO concentrations of 40 to 60 μM . After stabilization of the NO solution, the reduced enzyme was added to reach a final concentration of 7 μM . The current was monitored until it returned to zero.

N_2O Production Measurements. The production of N_2O by the two terminal oxidases was monitored using the $\nu(\text{NNO})$ stretch at 2230 cm^{-1} in their FTIR spectra (23). Protein solutions were made anaerobic by prolonged purging with argon on a Schlenk line and brought to a final enzyme concentration of 50 μM with 10 mM ascorbate and 0.1 mM TMPD in the glovebox. A diethylamine NONOate (Cayman Chemical, Ann Arbor, MI) stock solution, in 0.01 M NaOH, was prepared based on its $\epsilon_{250\text{ nm}} = 9180\text{ M}^{-1}\text{ cm}^{-1}$ extinction coefficient and an aliquot was used to confirm the concentration of the NO produced by monitoring the conversion of deoxymyoglobin to the nitrosyl complex. Quickly after the addition of NONOate to the protein solution, a 33 μL droplet of sample was deposited on a CaF_2 window and a second CaF_2 window was dropped on the sample. The optical path length was controlled by a 100 μm Teflon spacer. The FTIR cell was placed in the sample compartment of the FTIR instrument. FTIR spectra were obtained on a Perkin-Elmer system 2000 equipped with a liquid- N_2 -cooled MCT detector and purged with compressed air, dried, and depleted of CO_2 (Purge gas generator, puregas LLC). Sets of 100-scan accumulations were acquired every 2 min, at a 4 cm^{-1} resolution, until no further growth of the N_2O IR band was observed. These data were compared to a calibration curve obtained from solutions with varying N_2O concentrations.

EPR Experiments. EPR spectra were obtained on a Bruker E500 X-band EPR spectrometer equipped with a superX microwave bridge and a dual mode cavity with a helium flow cryostat (ESR900, Oxford Instruments, Inc.). The microwave power, modulation amplitude, magnetic field sweep, and the sample temperature were varied to optimize the detection of all potential EPR active species before and after illumination of the nitrosyl complexes.

RR Experiments. Typical enzyme concentrations used were 150 μM . The RR spectra were obtained using a custom McPherson 2061/207 spectrograph (set at 0.67 m with variable gratings) equipped with a Princeton Instruments liquid- N_2 -cooled CCD detector (LN-1100PB). Kaiser Optical supernotch filters were used to attenuate Rayleigh scattering generated by the 413 nm excitation of an Innova 302 krypton laser (Coherent, Santa Clara CA). Spectra were collected using a 90° scattering geometry on room-temperature samples mounted on a reciprocating translation stage. Frequencies were calibrated relative to indene and aspirin standards and are accurate to $\pm 1\text{ cm}^{-1}$. Polarization conditions were optimized using CCl_4 . The integrity of the RR samples, before and after illumination, was confirmed by direct monitoring of their UV–vis spectra in Raman capillaries.

FTIR Photolysis Experiments. FTIR photolysis experiments were carried out as previously described (17). After prolonged purging with argon on a Schlenk line, the sample was fully reduced by addition of 10 mM dithionite in an anaerobic glovebox. NO gas (^{14}NO from Airgas and Aldrich, ^{15}NO from ICON), initially treated with 1 M KOH solution,

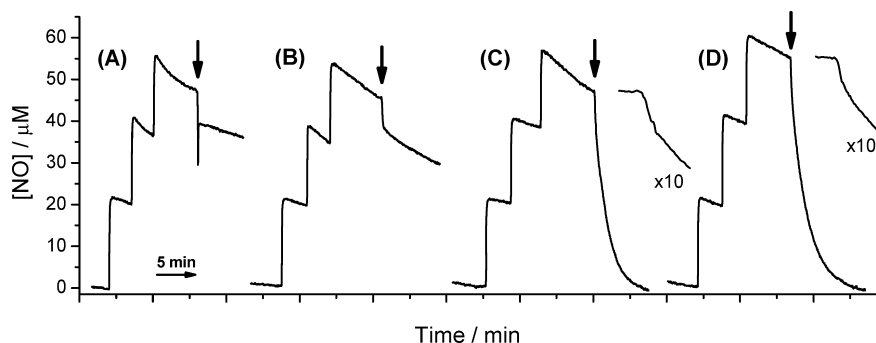


FIGURE 1: NO binding and reductase activity of ferrous myoglobin (A), aa_3 (B), ba_3 (C), and bo_3 (D) at 25 °C. Black arrows show time points where each enzyme was added (final concentration, 7 μ M). For ba_3 and bo_3 , the early part of the decay is also shown expanded 10-times to reveal the initial NO-binding step.

was added to the sample headspace to achieve an NO partial pressure of 0.1 atm. After 1 min of incubation at room temperature, 15 μ L of the protein solution was deposited as a droplet on a CaF₂ window and a second CaF₂ window was dropped on the sample using a 15 μ m Teflon spacer to complete the FTIR cell.

NO/CO mixed-gas experiments were carried out on \sim 350 μ M reduced-protein solutions containing 10 mM ascorbate, 0.1 mM TMPD, and 25% glycerol. The sample headspace was thoroughly exchanged with pure CO gas to reach saturation (¹²CO purchased from Airgas or ¹³CO purchased from ICON) and incubated for 15 min at room temperature. A few microliters of a stock solution of NONOate was added to the sample to produce 3.0 equiv of NO. Immediately after the addition of NONOate, a 15 μ L droplet of sample was deposited on a CaF₂ window with a 15 μ m Teflon spacer, and a second CaF₂ window was dropped on the sample to complete the IR cell. The 25% glycerol content of the sample ensured minimal degassing of CO during this procedure. Alternatively, the reduced protein (with the same concentration and buffer conditions as above) was exposed to a 0.1 atm NO partial pressure for 1 min and the headspace replaced with pure CO gas and incubated for 10 min at room temperature before transferring the sample to the IR cell.

For all samples, once the IR cell was securely sealed, the presence of the desired complexes was confirmed by obtaining a UV–vis spectrum of the sample using a Cary 50 spectrophotometer (Varian). The FTIR cell was then mounted to a closed-cycle cryogenic system (Displex, Advanced Research Systems) and placed in the sample compartment of the FTIR instrument to keep in the dark while the temperature dropped to 30 K. The temperature of the sample was monitored and controlled with a Cryo-Con 32 unit. Sets of 1000-scan accumulations were acquired at a 4 cm^{-1} resolution by the Perkin-Elmer system 2000. Photolysis of the nitrosyl and carbonyl complexes was achieved with continuous illumination of the sample directly in the FTIR sample chamber with a 50 W tungsten lamp after filtering out heat and NIR emission. This same illumination procedure was used to follow the dissociation and rebinding processes by UV–vis absorption spectroscopy with a Cary-50 spectrometer.

The reversibility of the photolysis events studied here was confirmed by comparing successive “dark” and “illuminated” UV–vis absorption spectra, and “dark” minus “illuminated” FTIR difference spectra obtained at 30 K after raising the temperature of the sample. A first evaluation of the temper-

ature dependence of the rebinding process was obtained by UV–vis absorption, raising the sample temperature incrementally by 10 K until the return of the “dark” spectrum was observed. The comparison of a first “dark” minus “illuminated” FTIR difference spectrum obtained at 30 K to a second 30 K difference spectra obtained after an incubation period at higher temperature, referred to below as the annealing temperature, provides a reliable means to compare rebinding-temperatures between distinct photolabile species.

RESULTS

NO Reductase Activity Measurements. While both ba_3 and bo_3 have been reported to possess NO reductase activity (12, 14), their steady-state turnover rates have not been compared in side-by-side experiments. Thus, we carried out parallel NO reductase activity measurements on ba_3 and bo_3 by monitoring NO consumption amperometrically under reducing conditions (10 mM ascorbate and 0.1 mM TMPD) (Figure 1). Upon addition of either myoglobin, aa_3 , ba_3 , or bo_3 to the NO solution, a rapid initial decay of current is assigned to the stoichiometric binding of NO to ferrous high-spin heme. While no further current change was observed with myoglobin or aa_3 , ba_3 and bo_3 displayed NO consumption with initial rates of 3.4 mol NO/mol ba_3 -min and 2.6 mol NO/mol bo_3 -min, respectively, at [NO] = 40 μ M (Figure 1). These values match that previously reported by Giuffrè et al. (3.0 ± 0.7 mol NO/mol ba_3 -min at [NO] = 55 μ M) (12) and complement the measurement by Butler et al. (0.3 mol NO/mol bo_3 -min at [NO] = 5 μ M) (14). It is worth noting that, in the presence of excess reducing agent, both enzymes remained as mononitrosyl complexes after the turnover measurements (data not shown). This observation indicates that, in both enzymes, the binding affinity for the second NO is much lower than that of the first NO.

The production of N₂O was monitored by the FTIR measurement of the antisymmetric N–N–O stretch mode ν_3 of N₂O at 2231 cm^{-1} . Using calibration curves with N₂O-saturated solutions, the 2231 cm^{-1} absorption values of the ba_3 and bo_3 solutions confirm that all of the NO consumed is converted to N₂O. (Figure S1 in the Supporting Information). As expected, N₂O was not detected in FTIR measurements when the terminal oxidases were replaced by myoglobin (data not shown).

UV–Vis, EPR and RR Characterization of bo_3 –NO. Exposure of fully reduced bo_3 to a headspace containing 0.1 atm of NO results in the rapid formation of bo_3 –NO. The

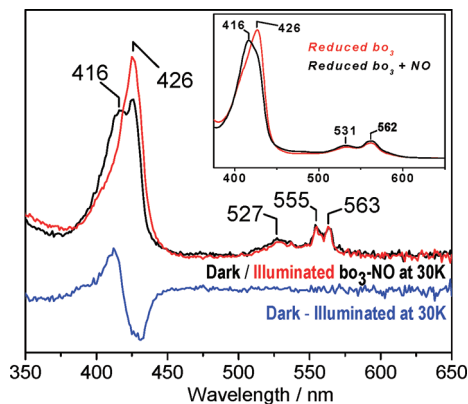


FIGURE 2: UV-vis spectra of bo_3 -NO complex at 30 K: dark (black), illuminated (red), and dark minus illuminated difference spectra (blue). The inset shows the room temperature UV-vis spectra of reduced bo_3 (red) and the bo_3 -NO complex (black).

Fe(II) heme o_3 Soret absorption at 426 nm is blue-shifted to generate a new Soret band at 416 nm, and there are only minor changes in the visible range of the room-temperature absorption spectra (Figure 2, inset). The Soret absorption at 416 nm, assigned to the heme o_3 -NO complex, is also observed at 30 K, but disappears following illumination (Figure 2). As reported previously (24), the EPR spectrum of the bo_3 -NO complex is characteristic of a 6-coordinate low-spin heme iron(II)-nitrosyl species with g values centered around 2 (2.102, 2.01, 1.99) and a nine-line ^{14}N -hyperfine structure ($A_{\text{NO}} = 20$ G, $A_{\text{His}} = 6$ G) equivalent to signals observed in ba_3 -NO (Figure S2 in the Supporting Information). In addition, this EPR spectrum includes an easily saturated, isotropic $g = 2.005$ with a 10 G line width which was previously assigned to a semiquinone radical (25, 26). Unlike the EPR features associated with the heme o_3 -NO, this signal is insensitive to short illumination at cryogenic temperatures (Figure S2 in the Supporting Information). The only new EPR signal observed after illumination is that of free NO at $g = 1.97$, which is best observed at high microwave power and below 10 K (data not shown).

RR spectra of the bo_3 -NO complex, obtained with a 413 nm excitation at room temperature, display enhancement of vibrational modes from the heme o_3 -NO complex (Figure 3). The porphyrin skeletal modes ν_4 , ν_3 , ν_2 , and ν_{10} at 1361, 1504, 1587, and 1638 cm^{-1} , respectively, are characteristic of a 6-coordinate low-spin heme-nitrosyl species. Vibrational modes involving the Fe-N-O unit are indentified by their $^{15}\text{N}^{18}\text{O}$ -downshifts (Figure 3). The $\nu(\text{N-O})_{o_3}$ mode is observed at 1615 cm^{-1} and exhibits a 67 cm^{-1} downshift with $^{15}\text{N}^{18}\text{O}$ that is within 5 cm^{-1} of the calculated shift for a diatomic N-O oscillator. Two bands, at 534 (-17) and 440 (-13) cm^{-1} , are assigned to $\nu(\text{Fe-NO})$ and $\delta(\text{Fe-NO})$ modes, respectively, even though significant mixing exists between these two modes (27-29). The unusually intense $\delta(\text{Fe-NO})$ band, which is not observed in ba_3 -NO (17, 30), and the low $\nu(\text{Fe-NO})$ frequency suggest that the Fe-N-O angle is smaller than the 140° equilibrium value. The low $\nu(\text{N-O})_{o_3}$ frequency is also consistent with a small Fe-N-O angle which favors the Fe(III)NO $^-$ resonance structure and N-O double-bond character.

Low-Temperature FTIR Photolysis of the bo_3 -NO and bo_3 -(NO)(CO) Complexes. Previously, we used photolysis experiments with ba_3 -NO at 30 K to isolate $\nu(\text{N-O})$

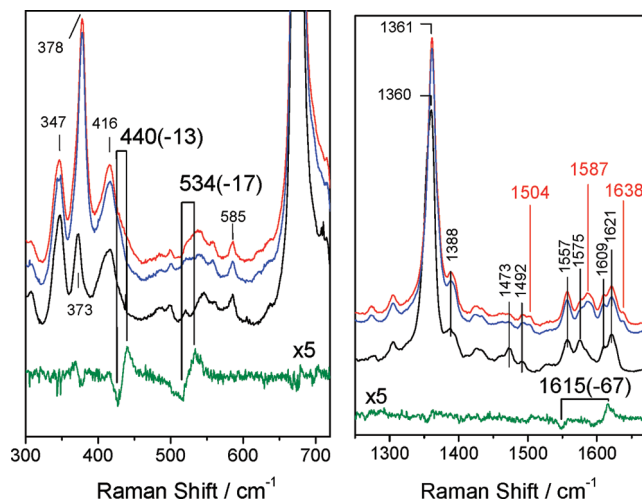


FIGURE 3: Low- and high-frequency RR spectra of bo_3 - $^{14}\text{N}^{16}\text{O}$ (red), bo_3 - $^{15}\text{N}^{18}\text{O}$ (blue), reduced bo_3 (black), and the bo_3 - $^{14}\text{N}^{16}\text{O}$ minus bo_3 - $^{15}\text{N}^{18}\text{O}$ difference spectrum (green) obtained with a 413 nm excitation at room temperature (protein concentration ~ 150 μM).

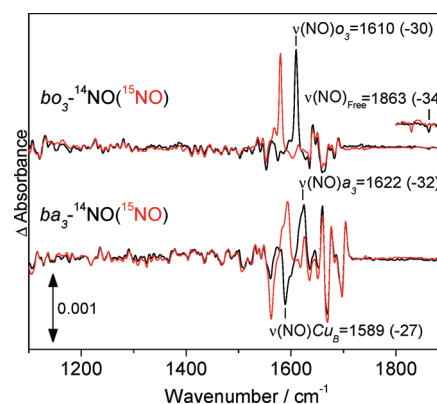


FIGURE 4: FTIR difference spectra ("dark" minus "illuminated") of bo_3 -NO (top traces) and ba_3 -NO (bottom traces) at 30 K. The spectra were obtained with protein concentrations ranging from 350 to 900 μM and were normalized based on the room temperature UV-vis spectra obtained directly from the FTIR cell (15 μm path length).

vibrations in "dark" minus "illuminated" FTIR difference spectra (17). These experiments revealed the disappearance of the $\nu(\text{N-O})_{a_3}$ at 1622 cm^{-1} , consistent with the dissociation of NO from the heme and accompanied by the formation of a Cu_B -nitrosyl complex with a negative $\nu(\text{N-O})_{\text{Cu}_B}$ at 1589 cm^{-1} . In the case of bo_3 -NO, the FTIR "dark" minus "illuminated" difference spectra show a sharp positive band at 1610 cm^{-1} that is readily assigned to the $\nu(\text{N-O})_{o_3}$ by its 30 cm^{-1} downshift with ^{15}NO , but there are no negative signals suggestive of a Cu_B -nitrosyl species (Figure 4). Instead, a negative band at 1863 cm^{-1} that shifts -34 cm^{-1} with ^{15}NO is characteristic of a $\nu(\text{N-O})$ from an NO molecule docked in a proteinaceous pocket, as observed with the nitrosyl complex of myoglobin (20). Varying buffer and salt conditions had no effect on the FTIR difference spectra of bo_3 -NO (Figure S3 in the Supporting Information). Thus, these experiments suggest that, despite the structural similarities of the heme-copper sites in these terminal oxidases (31, 32) and their efficient capture of photolyzed CO by $\text{Cu}_B(\text{I})$ in both terminal oxidases, NO transfer from heme to Cu_B does not occur in bo_3 . This interpretation is also supported by a difference between bo_3 -NO and ba_3 -NO in their temper-

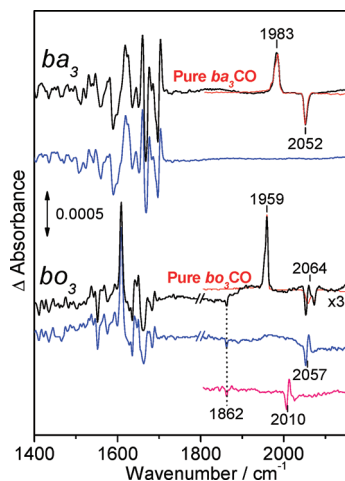


FIGURE 5: FTIR difference spectra (“dark” minus “illuminated”) of ba_3 -CO/NO (top) and bo_3 -CO/NO (bottom), before (black) and after annealing at 120 K (blue). Also shown for comparison, are the “dark” minus “illuminated” difference spectra for the pure-CO complexes (red traces) and the bo_3 - ^{13}CO /NO difference spectra after illumination and annealing at 120 K (pink). The spectra were obtained with protein concentrations near 350 μM and were normalized based on the room temperature UV-vis spectra obtained directly from the FTIR cell (15 μm path length).

ature dependence for geminate rebinding of NO. Indeed, after a first illumination at 30 K, the photolyzed ba_3 -NO complex must be annealed to 90 K to recover the full amplitude of the “dark” minus “illuminated” FTIR difference spectrum (17), whereas the temperature only needs to be raised to 60 K to allow for the complete rebinding of NO to heme o_3 in bo_3 -NO (data not shown).

To gain further insight into the catalytically relevant step in which two NO molecules interact with the heme-copper, and anticipating the formation of a nonreactive [(heme-copper)(NO)(CO)] tertiary complex, we carried out experiments on reduced ba_3 and bo_3 proteins with consecutive exposure to CO and NO gases. These experiments succeeded in forming a $[o_3\text{-NO}\cdot\text{OC-Cu}_B]$ complex in bo_3 (Figure 5). In ba_3 , exposure of ba_3 -CO, in the presence of excess CO, to 3 equiv of NO minutes before freezing (see Materials and Methods) resulted in the formation of ba_3 -NO and ba_3 -CO complexes that were easily distinguishable in the FTIR spectra (Figure 5). While rebinding of the photolyzed CO required annealing the sample above 220 K, the rebinding of NO was complete after annealing at 100 K. This difference in rebinding temperature allows for the separation of FTIR features associated with ba_3 -NO and ba_3 -CO. When the same experiment was carried out with bo_3 , features in the FTIR difference spectra associated with bo_3 -NO and bo_3 -CO complexes were also observed; however, the NO dissociation process induces a differential signal in the $\nu(\text{C-O})\text{Cu}_B$ region that shifts -47 cm^{-1} with ^{13}CO (Figure 5). We assign this signal, centered at 2057 cm^{-1} , to a perturbation of the Cu_B -carbonyl as NO is dissociated from heme o_3 . The $\nu(\text{NO})o_3$ in these mixed-gas experiments is observed at 1610 cm^{-1} and is indistinguishable from the $\nu(\text{NO})o_3$ observed when the complex is formed with pure NO. The relative intensities of the $\nu(\text{N-O})o_3$ and $\nu(\text{C-O})o_3$ bands suggest that the active site in the bo_3 -CO state represents only 10% of the sample, while the remaining 90% contains the heme o_3 -NO complex. Furthermore, on the basis of the $\nu(\text{C-O})\text{Cu}_B$ band observed in the “dark”

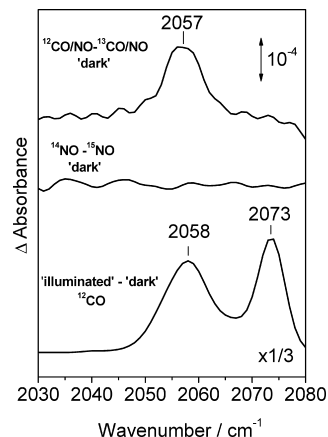


FIGURE 6: Comparison of FTIR difference spectra in the range of the $\nu(^{12}\text{C-O})\text{Cu}_B$ modes in bo_3 . From top to bottom: ^{12}CO minus ^{13}CO difference spectrum of “dark” bo_3 -CO/NO (top trace), ^{14}NO minus ^{15}NO difference spectrum of “dark” bo_3 -NO (middle trace), and “illuminated” minus “dark” bo_3 - ^{12}CO (bottom trace). The spectra were obtained with protein concentrations near 350 μM and were normalized based on the room temperature UV-vis spectra obtained directly from the FTIR cell (15 μm path length).

spectrum (Figure 6), we estimate that out of the 90% of nitrosylated active site, at least 10% binds CO to form the $[o_3\text{-NO}\cdot\text{OC-Cu}_B]$ complex. Thus, although the active site of bo_3 cannot bind two CO molecules at the same time, binding of NO to heme o_3 allows the subsequent binding of CO to Cu_B . The $\nu(\text{C-O})\text{Cu}_B$ band in the $[o_3\text{-NO}\cdot\text{OC-Cu}_B]$ complex is symmetric and centered at 2057 cm^{-1} , which contrasts the multiple conformers observed in the light-induced $[o_3\cdot\text{OC-Cu}_B]$ state (Figure 6). Changing the order of gas exposure by forming the heme-nitrosyl complexes before the addition of excess CO had no effect on the FTIR data obtained with bo_3 and ba_3 (data not shown).

DISCUSSION

Numerous studies with fully reduced terminal oxidases have shown that the five-coordinated ferrous high-spin heme efficiently binds NO to form a stable ferrous low-spin nitrosyl complex (33–38). Several terminal oxidases, including *T. thermophilus* ba_3 and *E. coli* bo_3 , have been shown to further react with a second NO molecule to catalyze the reduction of NO to N_2O (12, 14). Recently, we reported the formation of a photoinduced Cu_B -nitrosyl species with an end-on NO-Cu_B or a side-on Cu_B -nitrosyl configuration in ba_3 at cryogenic temperature (17) and proposed that this species reflects the binding geometry of the second NO molecule involved in the NO reductase reaction catalyzed by ba_3 (17). In the present work, we show that the bo_3 quinol oxidase from *E. coli* reduces NO at a rate equivalent to that of ba_3 ($\sim 3\text{ mol of NO/[E] mol}\cdot\text{min}$ at $[\text{NO}] = 40\text{ }\mu\text{M}$). In analogy to ba_3 , a stable 6-coordinate low-spin heme- o_3 nitrosyl complex is observed, which exhibits Fe-N-O stretching frequencies suggestive of a bent Fe-N-O geometry (27, 28). Illumination of bo_3 -NO at 30 K dissociates the heme-nitrosyl complex with equivalent efficiency as in ba_3 -NO, but complete rebinding of NO to the heme o_3 occurs after annealing the sample to 60 K, which is significantly lower than the 90 K annealing temperature measured in ba_3 -NO (17). Thus, the photolyzed bo_3 -NO state is thermodynamically less favored than the corresponding nitrosyl complex

in ba_3 . Comparison of low-temperature FTIR photolysis data for bo_3 -NO and ba_3 -NO support this conclusion. Indeed, light-induced FTIR difference spectra show that stabilization of the photolyzed NO through interactions with $Cu_B(I)$ does not occur in bo_3 -NO as it does in ba_3 -NO. Rather, the photolyzed FTIR spectra of bo_3 -NO reveals a $\nu(N-O)$ band at 1863 cm^{-1} which corresponds to an NO molecule docked in a proteinaceous pocket.

What prevents the formation of a light-induced Cu_B -nitrosyl in bo_3 ? Because the photolysis process with the bo_3 -CO complex leads to the efficient capture of the photolyzed CO by Cu_B , a lack of an open coordination site at Cu_B can be ruled out. Extensive RR and FTIR studies of heme-copper carbonyl complexes have revealed different configurations, which have been named α , β , and γ forms, that correspond to increasing levels of steric restrictions at the active site pocket (39–42). According to these studies, the ba_3 -CO complex represents a highly restricted site (γ form) (41), while the bo_3 -CO complex offers more open configurations of the dinuclear site (40). The iron-copper distances reported for the crystal structures of terminal oxidases concur with this view, with metal-metal distances ranging from 5.3 \AA in bo_3 to 4.4 \AA in ba_3 (31, 32, 43–46). However, metal-metal distance comparisons from crystal structures should be used with caution since the structure of bo_3 was only solved at 3.5 \AA resolution, and because the redox state of the active sites during the X-ray diffraction data acquisition is not always clearly defined. This point is exemplified by a recent X-ray crystallographic study of a surface double mutant of cytochrome ba_3 (E4Q and K258R) (47) which shows that the iron-copper distance can vary from 4.7 \AA in the X-ray photoreduced oxidized crystal to 5.05 \AA in chemically reduced crystals (48). However, the FTIR analysis of this double mutant in complexes with CO, NO, and NO in the presence of CO gas produced identical results to that of wild type ba_3 (Figures S4 and S5 in the Supporting Information).

Based on our FTIR results, we hypothesize that in bo_3 -NO, a larger metal-metal distance prevents the efficient capture of the photolyzed NO by Cu_B . This hypothesis also explains the formation of a bo_3 -(NO)(CO) complex which is not observed in ba_3 . This $[o_3\text{-NO}\cdot\text{OC-Cu}_B]$ state is evidenced by a differential signal centered at 2057 cm^{-1} from a Cu_B -carbonyl complex perturbed by the photolysis of NO from heme- o_3 . It is striking that one CO and one NO can coexist at the dinuclear site of bo_3 , while two CO molecules cannot (49). This observation suggests that the distance between heme o_3 and Cu_B is just large enough to accommodate one CO at the Cu_B with one NO at the heme o_3 in a bent geometry but not large enough to accommodate two linear diatomics. The limited accumulation of $[o_3\text{-NO}\cdot\text{OC-Cu}_B]$ to $\sim 12\%$ of the active sites may reflect the presence of multiple conformations of the heme-copper site (in bo_3). The $\nu(N-O)_{o_3}$ frequency in the $[o_3\text{-NO}\cdot\text{OC-Cu}_B]$ state is equivalent to that observed in the $[o_3\text{-NO}\cdot\text{Cu}_B]$ state. However, the $[o_3\text{-NO}\cdot\text{OC-Cu}_B]$ state exhibits only one $\nu(C-O)_{Cu_B}$ at 2057 cm^{-1} , which contrasts with the multiple $\nu(C-O)_{Cu_B}$ bands observed at 2058 and 2073 cm^{-1} after photolysis of bo_3 -CO at low temperature (Figure 6) (50, 51). EXAFS measurements suggest that high $\nu(C-O)_{Cu_B}$ frequencies could correspond to active site populations where one of the three coordinating histidines

to Cu_B is weakly bound (52). Regardless of the structural significance of the different $\nu(C-O)_{Cu_B}$ frequencies, the mixed-gas experiments suggest that the conformer that corresponds to the high $\nu(C-O)_{Cu_B}$ does not bind CO in the presence of the heme o_3 -NO complex.

Reports of concomitant binding of two diatomic molecules at heme-copper dinuclear sites are scarce. In fully reduced bovine and prokaryotic aa_3 , the loss or alteration of the EPR signal from a_3 -NO at high NO concentration has been assigned to the binding of a second NO molecule to Cu_B (35, 53). Using FTIR spectroscopy, Caughey and co-workers observed two $\nu(NO)$ s in bovine aa_3 : one at 1610 cm^{-1} assigned to a_3 -NO, and one at 1700 cm^{-1} assigned to Cu_B -NO (54). Presumably, the lack of NO reductase activity in aa_3 terminal oxidases permits the accumulation of a stable $[[FeNO]^7\cdot[CuNO]^{11}]$ complex, but the presence of two NO molecules in the active site of ba_3 and bo_3 is expected to represent a highly reactive intermediate within the NO reductase turnover. Although the characterization of a $[o_3\text{-NO}\cdot\text{OC-Cu}_B]$ complex in bo_3 suggests that this active site can also accommodate a $[[FeNO]^7\cdot[CuNO]^{11}]$ trans-complex, this state may also correspond to a dead-end adduct as in the aa_3 systems.

Low-temperature photolysis experiments are a sensitive probe of dinuclear heme-copper active sites. The results presented here show that fully reduced ba_3 and bo_3 bind a first NO molecule to the high-spin heme-iron(II) in similar fashion, but the distance of the Cu_B site relative to the heme iron differs significantly in the two proteins. In ba_3 , the close vicinity of the heme a_3 and the Cu_B allows for the transfer of the photolyzed NO from the heme to Cu_B in a side-on geometry (17). In bo_3 , the larger metal-metal distance does not restrict the coordination of a second diatomic molecule at the Cu_B site, as long as it can adopt a bent geometry. Our experiments do not determine whether the $Cu_B(I)$ site in bo_3 -NO binds a second NO molecule to form a trans $[[FeNO]^7\cdot[CuNO]^{11}]$ complex. Nevertheless, the comparison of ba_3 and bo_3 shows that the mechanism of NO reduction can accommodate the difference in heme-copper distances in these two active sites. This conclusion argues against the coordination of the second NO molecule to $Cu_B(I)$ as an essential step in the reaction mechanism. Instead, the role of the Cu_B site may be limited to promote the formation of a heme iron-hyponitrite species through electrostatic interactions (11, 16).

ACKNOWLEDGMENT

We thank Dr. Ninian Blackburn for the use of his Clark electrode, and Dr. James Whittaker for the use of his liquid helium cryostat.

SUPPORTING INFORMATION AVAILABLE

FTIR spectra monitoring N_2O production, EPR spectra of the bo_3 -NO complex, FTIR spectra of bo_3 -NO at different pH and salt concentrations, and comparison of FTIR data for ba_3 wild type and double mutant E4Q/K258R. This material is available free of charge via the Internet at <http://pubs.acs.org>.

REFERENCES

1. Lissenden, S., Mohan, S., Overton, T., Regan, T., Crooke, H., Cardinale, J. A., Householder, T. C., Adams, P., O'connor, C. D.,

- Clark, V. L., Smith, H., and Cole, J. A. (2000) Identification of transcription activators that regulate gonococcal adaptation from aerobic to anaerobic or oxygen-limited growth. *Mol. Microbiol.* 37, 839–855.
2. Householder, T. C., Fozo, E. M., Cardinale, J. A., and Clark, V. L. (2000) Gonococcal nitric oxide reductase is encoded by a single gene, norB, which is required for anaerobic growth and is induced by nitric oxide. *Infect. Immun.* 68, 5241–5246.
3. Anjum, M. F., Stevanin, T. M., Read, R. C., and Moir, J. W. (2002) Nitric oxide metabolism in *Neisseria meningitidis*. *J. Bacteriol.* 184, 2987–2993.
4. Castresana, J., Lubben, M., Saraste, M., and Higgins, D. G. (1994) Evolution of cytochrome oxidase, an enzyme older than atmospheric oxygen. *EMBO J.* 13, 2516–2525.
5. Zumft, W. G., Braun, C., and Cuyper, H. (1994) Nitric oxide reductase from *Pseudomonas stutzeri*. Primary structure and gene organization of a novel bacterial cytochrome bc complex. *Eur. J. Biochem.* 219, 481–490.
6. van der Oost, J., de Boer, A. P., de Gier, J. W., Zumft, W. G., Stouthamer, A. H., and van Spanning, R. J. (1994) The heme-copper oxidase family consists of three distinct types of terminal oxidases and is related to nitric oxide reductase. *FEMS Microbiol. Lett.* 121, 1–9.
7. Heiss, B., Frunzke, K., and Zumft, W. G. (1989) Formation of the N–N bond from nitric oxide by a membrane-bound cytochrome bc complex of nitrate-respiring (denitrifying) *Pseudomonas stutzeri*. *J. Bacteriol.* 171, 3288–3297.
8. Averill, B. A. (1996) Dissimilatory nitrite and nitric oxide reductases. *Chem. Rev.* 96, 2951–2965.
9. Wasser, I. M., de Vries, S., Moëne-Loccoz, P., Schroder, I., and Karlin, K. D. (2002) Nitric oxide in biological denitrification: Fe/Cu metalloenzyme and metal complex NO_x redox chemistry. *Chem. Rev.* 102, 1201–1234.
10. Zumft, W. G. (2005) Nitric oxide reductases of prokaryotes with emphasis on the respiratory, heme-copper oxidase type. *J. Inorg. Biochem.* 99, 194–215.
11. Moëne-Loccoz, P. (2007) Spectroscopic characterization of heme iron-nitrosyl species and their role in NO reductase mechanisms in diiron proteins. *Nat. Prod. Rep.* 24, 610–620.
12. Giuffrè, A., Stubauer, G., Sarti, P., Brunori, M., Zumft, W. G., Buse, G., and Soulimane, T. (1999) The heme-copper oxidases of *Thermus thermophilus* catalyze the reduction of nitric oxide: evolutionary implications. *Proc. Natl. Acad. Sci. U.S.A.* 96, 14718–14723.
13. Forte, E., Urbani, A., Saraste, M., Sarti, P., Brunori, M., and Giuffrè, A. (2001) The cytochrome cbb₃ from *Pseudomonas stutzeri* displays nitric oxide reductase activity. *Eur. J. Biochem.* 268, 6486–6491.
14. Butler, C., Forte, E., Maria Scandurra, F., Arese, M., Giuffrè, A., Greenwood, C., and Sarti, P. (2002) Cytochrome bo₃ from *Escherichia coli*: the binding and turnover of nitric oxide. *Biochem. Biophys. Res. Commun.* 296, 1272–1278.
15. Ohta, T., Kitagawa, T., and Varotsis, C. (2006) Characterization of a bimetallic-bridging intermediate in the reduction of NO to N₂O: a density functional theory study. *Inorg. Chem.* 45, 3187–3190.
16. Blomberg, M. L., Blomberg, M. R. A., and Siegbahn, P. E. M. (2006) A theoretical study of nitric oxide reductase activity in a ba₃-type heme-copper oxidase. *Biochim. Biophys. Acta* 1757, 31–46.
17. Hayashi, T., Lin, I. J., Chen, Y., Fee, J. A., and Moëne-Loccoz, P. (2007) Fourier transform infrared characterization of a Cu_B-nitrosyl complex in cytochrome ba₃ from *Thermus thermophilus*: relevance to NO reductase activity in heme-copper terminal oxidases. *J. Am. Chem. Soc.* 129, 14952–14958.
18. Pilet, E., Nitschke, W., Rappaport, F., Soulimane, T., Lambry, J. C., Liebl, U., and Vos, M. H. (2004) NO binding and dynamics in reduced heme-copper oxidases aa₃ from *Paracoccus denitrificans* and ba₃ from *Thermus thermophilus*. *Biochemistry* 43, 14118–14127.
19. Butler, C. S., Seward, H. E., Greenwood, C., and Thomson, A. J. (1997) Fast cytochrome bo from *Escherichia coli* binds two molecules of nitric oxide at Cu_B. *Biochemistry* 36, 16259–16266.
20. Miller, L. M., Pedraza, A. J., and Chance, M. R. (1997) Identification of conformational substates involved in nitric oxide binding to ferric and ferrous myoglobin through difference Fourier transform infrared spectroscopy (FTIR). *Biochemistry* 36, 12199–12207.
21. Chen, Y., Hunsicker-Wang, L., Pacoma, R. L., Luna, E., and Fee, J. A. (2005) A homologous expression system for obtaining engineered cytochrome ba₃ from *Thermus thermophilus* HB8. *Protein Expression Purif.* 40, 299–318.
22. Rumbley, J. N., Furlong Nickels, E., and Gennis, R. B. (1997) One-step purification of histidine-tagged cytochrome bo₃ from *Escherichia coli* and demonstration that associated quinone is not required for the structural integrity of the oxidase. *Biochim. Biophys. Acta* 1340, 131–142.
23. Zhao, X. J., Sampath, V., and Caughey, W. S. (1995) Cytochrome c oxidase catalysis of the reduction of nitric oxide to nitrous oxide. *Biochem. Biophys. Res. Commun.* 212, 1054–1060.
24. Cheesman, M. R., Watmough, N. J., Pires, C. A., Turner, R., Brittain, T., Gennis, R. B., Greenwood, C., and Thomson, A. J. (1993) Cytochrome bo from *Escherichia coli*: identification of haem ligands and reaction of the reduced enzyme with carbon monoxide. *Biochem. J.* 289, 709–718.
25. Yap, L. L., Samoilova, R. I., Gennis, R. B., and Dikanov, S. A. (2007) Characterization of mutants that change the hydrogen bonding of the semiquinone radical at the Q_H site of the cytochrome bo₃ from *Escherichia coli*. *J. Biol. Chem.* 282, 8777–8775.
26. Yap, L. L., Samoilova, R. I., Gennis, R. B., and Dikanov, S. A. (2006) Characterization of the exchangeable protons in the immediate vicinity of the semiquinone radical at the Q_H site of the cytochrome bo₃ from *Escherichia coli*. *J. Biol. Chem.* 281, 16879–16887.
27. Coyle, C. M., Vogel, K. M., Rush, T. S., 3rd, Kozlowski, P. M., Williams, R., Spiro, T. G., Dou, Y., Ikeda-Saito, M., Olson, J. S., and Zgierski, M. Z. (2003) FeNO structure in distal pocket mutants of myoglobin based on resonance Raman spectroscopy. *Biochemistry* 42, 4896–4903.
28. Ibrahim, M., Xu, C., and Spiro, T. G. (2006) Differential sensing of protein influences by NO and CO vibrations in heme adducts. *J. Am. Chem. Soc.* 128, 16834–16845.
29. Xu, C., and Spiro, T. G. (2008) Ambidentate H-bonding by heme-bound NO: structural and spectral effects of -O versus -N H-bonding. *J. Biol. Inorg. Chem.* 613–621.
30. Pinakoulaki, E., Ohta, T., Soulimane, T., Kitagawa, T., and Varotsis, C. (2005) Detection of the His-heme Fe²⁺-NO species in the reduction of NO to N₂O by ba₃-oxidase from *Thermus thermophilus*. *J. Am. Chem. Soc.* 127, 15161–15167.
31. Soulimane, T., Buse, G., Bourenkov, G. P., Bartunik, H. D., Huber, R., and Than, M. E. (2000) Structure and mechanism of the aberrant ba₃-cytochrome c oxidase from *Thermus thermophilus*. *EMBO J.* 19, 1766–1776.
32. Abramson, J., Riistama, S., Larsson, G., Jasaitis, A., Svensson-Ek, M., Laakkonen, L., Puustinen, A., Iwata, S., and Wikstrom, M. (2000) The structure of the ubiquinol oxidase from *Escherichia coli* and its ubiquinone binding site. *Nat. Struct. Biol.* 7, 910–917.
33. Blokzijl-Homan, M. F., and van Gelder, B. F. (1971) Biochemical and biophysical studies on cytochrome aa₃. 3. The EPR spectrum of NO-ferrocycytochrome a₃. *Biochim. Biophys. Acta* 234, 493–498.
34. Stevens, T. H., Brudvig, G. W., Bocian, D. F., and Chan, S. I. (1979) Structure of cytochrome a₃-Cu_{a3} couple in cytochrome c oxidase as revealed by nitric oxide binding studies. *Proc. Natl. Acad. Sci. U.S.A.* 76, 3320–3324.
35. Brudvig, G. W., Stevens, T. H., and Chan, S. I. (1980) Reactions of nitric oxide with cytochrome c oxidase. *Biochemistry* 19, 5275–5285.
36. Mascarenhas, R., Wei, Y. H., Scholes, C. P., and King, T. E. (1983) Interaction in cytochrome c oxidase between cytochrome a₃ ligated with nitric oxide and cytochrome a. *J. Biol. Chem.* 258, 5348–5351.
37. Blackmore, R. S., Greenwood, C., and Gibson, Q. H. (1991) Studies of the primary oxygen intermediate in the reaction of fully reduced cytochrome oxidase. *J. Biol. Chem.* 266, 19245–19249.
38. Vos, M. H., Lipowski, G., Lambry, J. C., Martin, J. L., and Liebl, U. (2001) Dynamics of nitric oxide in the active site of reduced cytochrome c oxidase aa₃. *Biochemistry* 40, 7806–7811.
39. Alben, J. O., Moh, P. P., Fiamingo, F. G., and Altschuld, R. A. (1981) Cytochrome oxidase a₃ heme and copper observed by low-temperature Fourier transform infrared spectroscopy of the CO complex. *Proc. Natl. Acad. Sci. U.S.A.* 78, 234–237.
40. Puustinen, A., Bailey, J. A., Dyer, R. B., Mecklenburg, S. L., Wikstrom, M., and Woodruff, W. H. (1997) Fourier transform infrared evidence for connectivity between Cu_B and glutamic acid 286 in cytochrome bo₃ from *Escherichia coli*. *Biochemistry* 36, 13195–13200.
41. Einarsdottir, O., Killough, P. M., Fee, J. A., and Woodruff, W. H. (1989) An infrared study of the binding and photodissociation of

- carbon monoxide in cytochrome *ba*₃ from *Thermus thermophilus*. *J. Biol. Chem.* 264, 2405–2408.
42. Wang, J., Takahashi, S., Hosler, J. P., Mitchell, D. M., Ferguson-Miller, S., Gennis, R. B., and Rousseau, D. L. (1995) Two conformations of the catalytic site in the *aa*₃-type cytochrome *c* oxidase from *Rhodobacter sphaeroides*. *Biochemistry* 34, 9819–9825.
 43. Iwata, S., Ostermeier, C., Ludwig, B., and Michel, H. (1995) Structure at 2.8 Å resolution of cytochrome *c* oxidase from *Paracoccus denitrificans*. *Nature* 376, 660–669.
 44. Yoshikawa, S., Shinzawa-Itoh, K., Nakashima, R., Yaono, R., Yamashita, E., Inoue, N., Yao, M., Fei, M. J., Libeu, C. P., Mizushima, T., Yamaguchi, H., Tomizaki, T., and Tsukihara, T. (1998) Redox-coupled crystal structural changes in bovine heart cytochrome *c* oxidase. *Science* 280, 1723–1729.
 45. Tsukihara, T., Aoyama, H., Yamashita, E., Tomizaki, T., Yamaguchi, H., Shinzawa, I.-K., Nakashima, R., Yaono, R., and Yoshikawa, S. (1996) The whole structure of the 13-subunit oxidized cytochrome *c* oxidase at 2.8 Å. *Science* 272, 1136–1144.
 46. Hunsicker-Wang, L. M., Pacoma, R. L., Chen, Y., Fee, J. A., and Stout, C. D. (2005) A novel cryoprotection scheme for enhancing the diffraction of crystals of recombinant cytochrome *ba*₃ oxidase from *Thermus thermophilus*. *Acta Crystallogr. D* 61, 340–343.
 47. Liu, B., Luna, V. M., Chen, Y., Stout, C. D., and Fee, J. A. (2007) An unexpected outcome of surface engineering an integral membrane protein: improved crystallization of cytochrome *ba*₃ from *Thermus thermophilus*. *Acta Crystallogr. F* 63, 1029–1034.
 48. Liu, B., Chen, Y., Doukov, T., Soltis, S. M., Stout, C. D., and Fee, J. A. (2008) Combined microspectroscopic and crystallographic examination of chemically-reduced and X-ray radiation-reduced forms of cytochrome *ba*₃ oxidase from *Thermus thermophilus*: structure of the reduced form of the enzyme. *Biochemistry*, in press.
 49. We confirmed that the conditions used to accumulate a *bo*₃-(NO)(CO) complex (1 atm of CO, 25% glycerol, 30 K) do not allow for the formation of a *bo*₃-(CO)₂ complex in the absence of NO gas. Specifically, the low-temperature UV-vis and FTIR spectra show full complexation of the heme *o*₃ by CO and complete transfer of CO from *o*₃ to Cu_B upon illumination, with carbonyl stretching frequencies and intensities that are indistinguishable from those observed at low CO concentrations with 5% glycerol. In contrast with the terminal oxidases, the active site of the NO reductase from *Bacillus azotoformans* was shown to bind two CO molecules: Lu, S., Suharti, de Vries, S., and Moënné-Loccoz, P. (2004) Two CO molecules can bind concomitantly at the diiron site of NO reductase from *Bacillus azotoformans*. *J. Am. Chem. Soc.* 126, 15332–15333.
 50. Hill, J., Goswitz, V. C., Calhoun, M., Garcia-Horsman, J. A., Lemieux, L., Alben, J. O., and Gennis, R. B. (1992) Demonstration by FTIR that the *bo*-type ubiquinol oxidase of *Escherichia coli* contains a heme-copper binuclear center similar to that in cytochrome *c* oxidase and that proper assembly of the binuclear center requires the *cyoE* gene product. *Biochemistry* 31, 11435–11440.
 51. Calhoun, M. W., Lemieux, L. J., Thomas, J. W., Hill, J. J., Goswitz, V. C., Alben, J. O., and Gennis, R. B. (1993) Spectroscopic characterization of mutants supports the assignment of histidine-419 as the axial ligand of heme *o* in the binuclear center of the cytochrome *bo* ubiquinol oxidase from *Escherichia coli*. *Biochemistry* 32, 13254–13261.
 52. Ralle, M., Verkhovskaya, M. L., Morgan, J. E., Verkhovsky, M. I., Wikstrom, M., and Blackburn, N. J. (1999) Coordination of Cu_B in reduced and CO-liganded states of cytochrome *bo*₃ from *Escherichia coli*. Is chloride ion a cofactor? *Biochemistry* 38, 7185–7194.
 53. Pilet, E., Nitschke, W., Liebl, U., and Vos, M. H. (2007) Accommodation of NO in the active site of mammalian and bacterial cytochrome *c* oxidase *aa*₃. *Biochim. Biophys. Acta* 1767, 387–392.
 54. Zhao, X. J., Sampath, V., and Caughey, W. S. (1994) Infrared characterization of nitric oxide bonding to bovine heart cytochrome *c* oxidase and myoglobin. *Biochem. Biophys. Res. Commun.* 204, 537–543.

BI801915R